AFRL-RV-PS-
TR-2023-0150

AFRL-RV-PS-
TR-2023-0150

EARTHQUAKE SIGNAL CHARACTERIZATION USING DEEP-RESIDUAL CONVOLUTIONAL-RECURRENT NETWORKS

Gregory C. Beroza

Leland Stanford Junior University
The Stanford University
Department of Geophysics
397 Panama Mall
Stanford, CA 94305-2215

26 November 2023

Final Report

AIR FORCE RESEARCH LABORATORY
Space Vehicles Directorate
3550 Aberdeen Ave SE
AIR FORCE MATERIEL COMMAND
KIRTLAND AIR FORCE BASE, NM 87117-5776

DTIC COPY

NOTICE AND SIGNATURE PAGE

AFRL-RV-PS-TR-2023-0150 HAS BEEN REVIEWED AND IS APPROVED FOR PUBLICATION IN ACCORDANCE WITH ASSIGNED DISTRIBUTION STATEMENT.

//SIGNED//	//SIGNED//
_____	_____
Ist Lt. Simone E. Smith	Mark E. Roverse, Chief
Program Manager/AFRL/RVB	AFRL Geospace Technologies Division

This report is published in the interest of scientific and technical information exchange, and its publication does not constitute the Government's approval or disapproval of its ideas or findings.

REPORT DOCUMENTATION PAGE

Form Approved
OMB No. 0704-0188

1. REPORT DATE *(DD-MM-YYYY)*	**2. REPORT TYPE**	**3. DATES COVERED** *(From - To)*
26-11-2023	Final Report	23 Sep 2019 – 20 Sep 2023

4. TITLE AND SUBTITLE
Earthquake Signal Characterization Using Deep-Residual Convolutional-Recurrent Networks

5a. CONTRACT NUMBER
FA9453-19-C-0073

5b. GRANT NUMBER

5c. PROGRAM ELEMENT NUMBER
C6601F

6. AUTHOR(S)
Gregory C. Beroza

5d. PROJECT NUMBER
1010

5e. TASK NUMBER
EF134033

5f. WORK UNIT NUMBER
V1GZ

7. PERFORMING ORGANIZATION NAME(S) AND ADDRESS(ES)
Leland Stanford Junior University
The Stanford University
Department of Geophysics
397 Panama Mall
Stanford, CA 94305-2215

8. PERFORMING ORGANIZATION REPORT NUMBER

9. SPONSORING / MONITORING AGENCY NAME(S) AND ADDRESS(ES)
Air Force Research Laboratory
Space Vehicles Directorate
3550 Aberdeen Avenue SE
Kirtland AFB, NM 87117-5776

10. SPONSOR/MONITOR'S ACRONYM(S)
AFRL/RVBN

11. SPONSOR/MONITOR'S REPORT NUMBER(S)
AFRL-RV-PS-TR-2023-0150

12. DISTRIBUTION / AVAILABILITY STATEMENT
Approved for public release; distribution is unlimited (AFRL-2023-6424 dtd 27 Dec 2023).

13. SUPPLEMENTARY NOTES

14. ABSTRACT
Advances in deep learning have led to a surge of interest in machine learning for the constituent tasks of seismic monitoring. Seismic waveforms are strongly non-stationary, and the waveforms that seismic sources produce are complex, with spatial and temporal behaviors that reflect complexity in the sources that generate seismic waves and in the medium that those waves propagate through. New approaches can exploit these complex data more fully than conventional approaches. Under this contract we developed and demonstrated multiple new and innovative signal characterization methods based on deep learning of local and regional seismic data to improve seismic event detection.

15. SUBJECT TERMS
seismic signal detection, seismic association, seismic magnitude, seismic phase identification, machine learning and seismology, deep learning and seismology

16. SECURITY CLASSIFICATION OF:			**17. LIMITATION OF ABSTRACT**	**18. NUMBER OF PAGES**	**19a. NAME OF RESPONSIBLE PERSON**
a. REPORT	**b. ABSTRACT**	**c. THIS PAGE**			1st Lt. Simone E. Smith
Unclassified	Unclassified	Unclassified	Unlimited	36	**19b. TELEPHONE NUMBER** *(include area code),*

This page is intentionally left blank.

TABLE OF CONTENTS

Section **Page**

LIST OF FIGURES

Figure **Page**

LIST OF FIGURES (continued)

Figure **Page**

This page is intentionally left blank.

1. SUMMARY

Advances in deep learning have led to a surge of interest in machine learning for the constituent tasks of seismic monitoring. Seismic waveforms are strongly non-stationary, and those waveforms are complex, with spatial and temporal behaviors that reflect complexity in the sources that generate seismic waves and in the medium that those waves propagate through. New approaches can exploit these complex data more fully than conventional approaches. Under this contract we developed and demonstrated multiple new and innovative signal characterization methods based on deep learning of local and regional seismic data to improve seismic event detection.

2. INTRODUCTION

Seismic monitoring is the task of detecting signals from earthquakes or other impulsive/transient seismic sources in continuous waveform data to develop a catalog of seismic sources and to determine their source characteristics. Under this project we have developed multiple deep learning methods that can be deployed to improve the performance of tasks within seismic monitoring workflows. We have also developed a scalable, cloud-based machine learning workflow that can be deployed for either realtime monitoring or for mining the very largest archived waveform data sets. These methods allow fast, effective, and accurate detection that often results in an order of magnitude, and sometimes more, small events than are present in catalogs developed with conventional approaches.

3. TECHNICAL APPROACH

3.1 Machine Learning for Earthquake Detection

Direct detection of seismic events in waveform time series can be accomplished through normalized cross correlation of known event waveforms known as template matching (*Gibbons and Ringdal*, 2006). When event templates are *a priori* incompletely known, or even entirely unknown, uninformed search can be used to identify repeating sources, but this rapidly becomes computationally challenging (*Brown et al*., 2008). In such cases, the data-mining approach of set-based similarity search can be used to identify repeating signals using locality-sensitive hashing (*Yoon et al.,* 2015). The promise of machine learning for event detection is that it could generalize similarity search from strict wiggle-for-wiggle waveform similarity, to similarity based on waveform features, where "features" represent more general characteristics of seismic waveforms.

3.1.1 CRED: A Convolutional-Recurrent Earthquake Detector. We realized this promise with a first-generation machine-learning based seismic event detection algorithm that we called Convolutional-Recurrent Earthquake Detector or CRED (*Mousavi et al.,* 2019a). CRED uses a combination of convolutional layers and bi-directional long-short-term memory units (Fig. 1). It learns time-frequency characteristics of the dominant phases

in an earthquake signal from three component data recorded on individual stations. We trained the network using 500,000 seismograms (250k associated with tectonic earthquakes and 250k identified as noise) as recorded by the Northern California Seismic Network and demonstrated the performance of the trained model by applying it to a set of semi-synthetic signals. We also applied the model to one month of continuous data recorded in Central Arkansas to demonstrate its efficiency, sensitivity, and ability to generalize. In that setting, CRED detected more than 800 induced microearthquakes as small as M_L −1.3. We compared the performance of the model with the STA/LTA, template matching, and FAST algorithms, and concluded that this approach held great promise for lowering the detection threshold, generalizing from similarity search, while minimizing false positive detections. Figure 2 shows several examples of CRED output for a variety of seismic event waveforms.

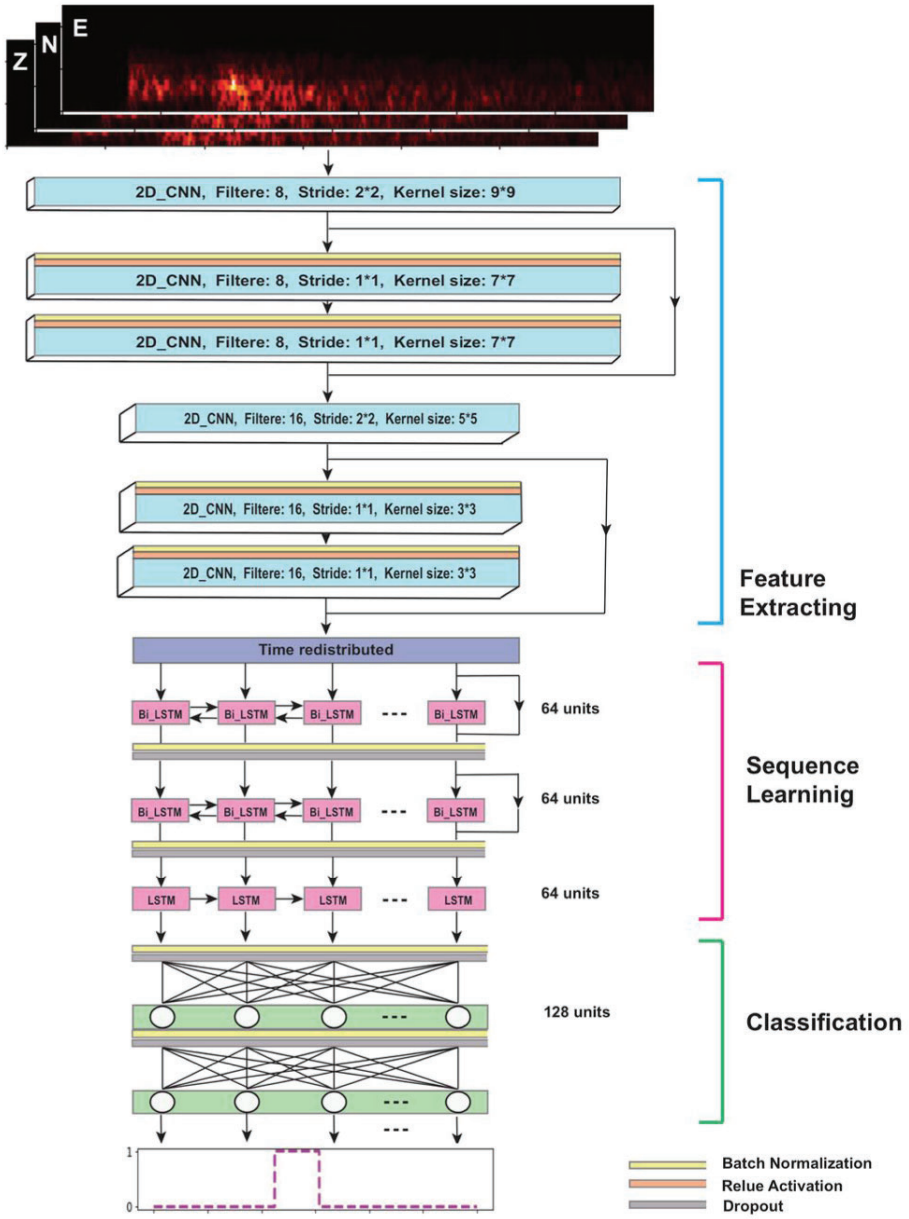

Figure 1. **Schematic of architecture of the CRED convolutional-recurrent earthquake detector.** *Model input is time-frequency representation of three-component waveform data and output is the binary classification probability of event vs. non-event.*

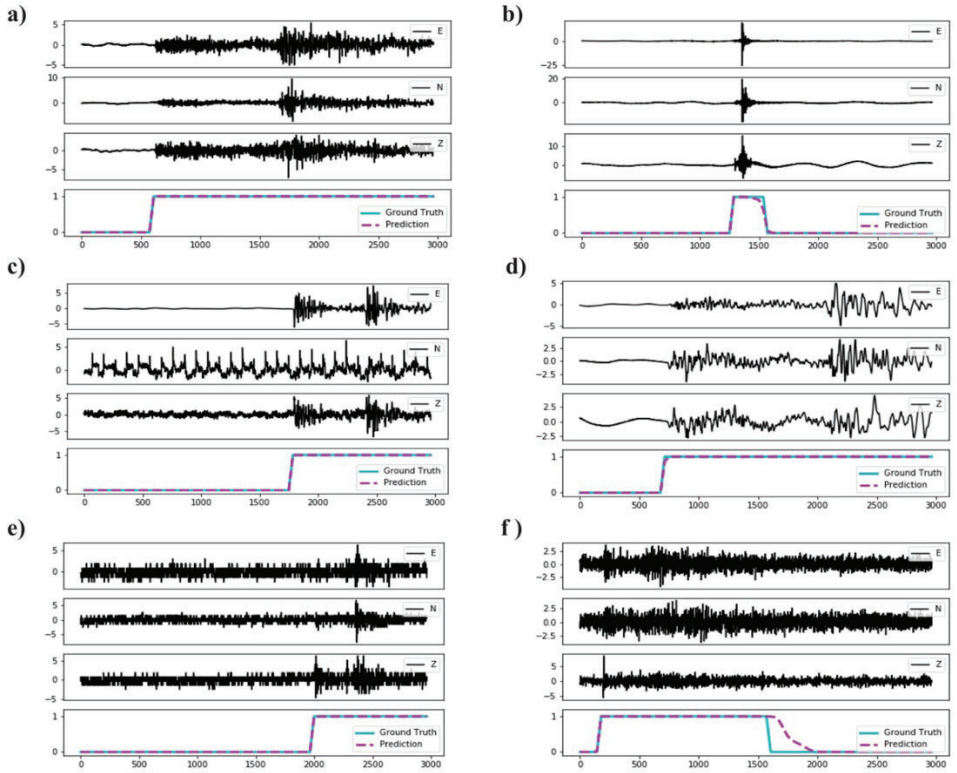

Figure 2. **Results of applying the trained network on six samples from the test set.** *In each case the upper three sub-panels are the corresponding waveform time series and final panel compares output classification vs. ground truth.*

CRED combines convolutional and recurrent units for deep residual learning of the time-frequency characteristics of earthquake signals. It detects seismic events with high efficiency and precision, and with manageably low sensitivity to background noise and a tolerable false positive rate. We found that it generalized well to out of distribution data consisting of induced earthquake sequences in Arkansas for which events tend to be smaller in magnitude, shallower in depth, and that occur in a different tectonic and geologic environment than the Northern California data set that the model was trained on. Application is efficient once the network is trained such that it can be applied to a stream of seismic data in real time.

3.1.2 EQTransformer: An Attentive, Multi-Task Detector. During the second year of the project we published a successor to CRED that we call EQTransformer (*Mousavi et al.,* 2020). EQTransformer is a multi-task model that simultaneously detects earthquake signals and measures seismic-phase arrival times. Performing these two related tasks in tandem improves model performance in each individual task by combining information in phases and on the full waveform of earthquake signals.

Earthquake detection and arrival time measurement are both aspects of seismic event detection and have commonalities, but their objectives are not quite the same. Minimizing the false negative and false positive rates is the primary goal in detection; however, in phase picking false positives are less of a problem because they can be sorted out in the phase association process. Phase picking also brings with it the importance of temporal accuracy due to the sensitivity of location estimates to arrival time measurements (0.1 second of error in determining P-wave arrivals can translate to hundreds of meters of location error). In the other words, with respect to waveform data, phase picking is more of a local problem compared to the detection, which benefits from a more global view and effectively considers multiple seismic phase arrivals that include the scattered waves of the coda.

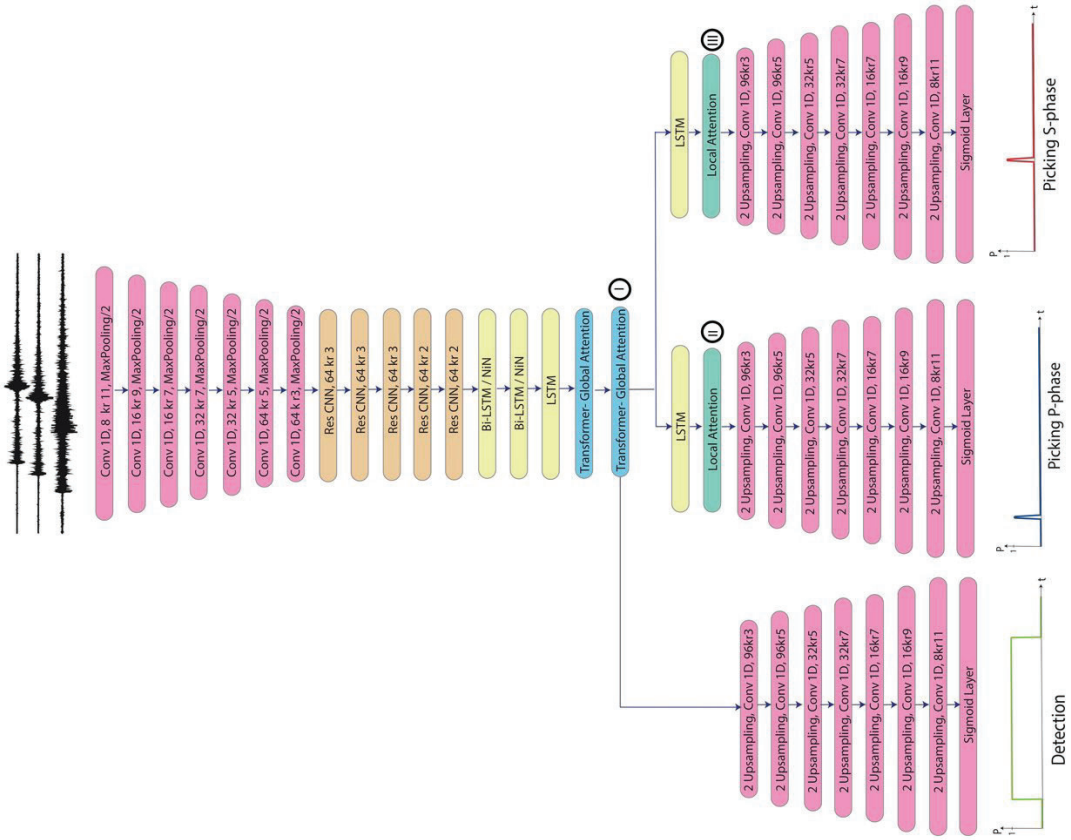

Figure 3. **Architecture of EQTransformer.** *The multi-task architecture is designed to consider an input 3-component seismogram and produce three outputs: (1) detection of an earthquake/not an earthquake; (2) P-wave pick; and (3) S-wave pick. By combining these tasks in a single network, the model uses both the local phase information and global earthquake waveform information to improve the performance of each.*

Previous machine-learning studies approached these tasks individually using separate networks; however, because these tasks are related there are benefits to considering them together. This approach mimics seismic analysts' practice of using the entire waveform context to identify consistent elements of an earthquake signal (e.g. P, S, coda and surface waves) with a specific ordering (P-wave always arrives before S-wave, higher frequency body waves always precede dispersive surface waves etc.) to determine whether or not a

signal is from an earthquake. They then focus on each phase to precisely pick the arrival times. This practice indicates the interconnection of these two tasks and the importance of contextual information in earthquake signal modeling. Additional context could come from multiple stations (*Zhu et al.,* 2022) or the occurrence of multiple similar events closely spaced in time, such as during an aftershock sequence (*Kværna et al.,* 2023).

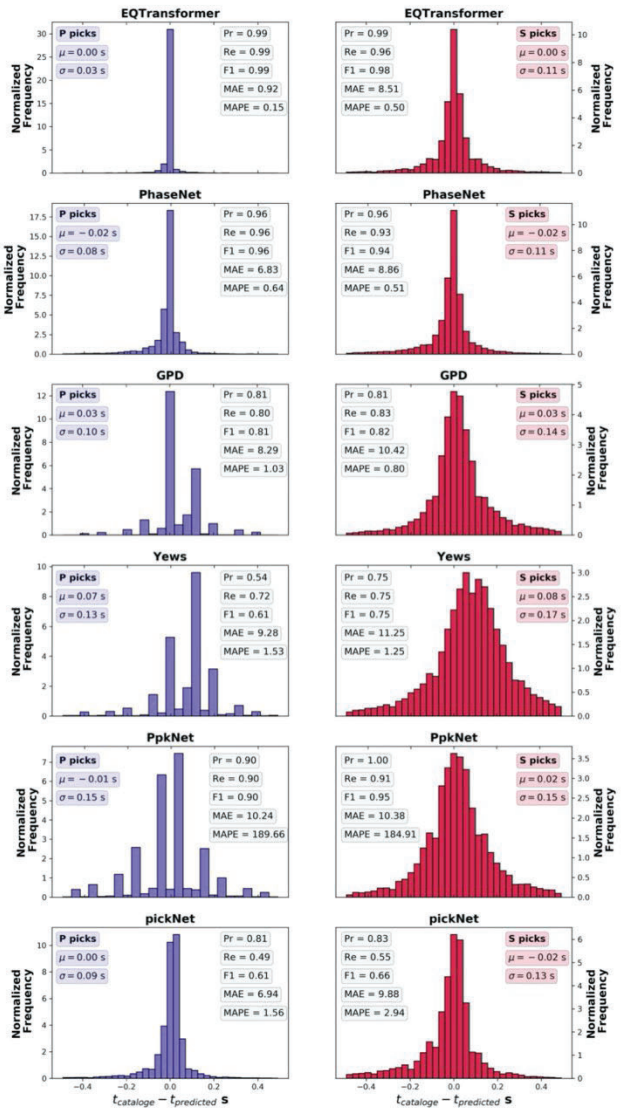

Figure 4. **Comparison of picking accuracy.** *(P on the left and S on the right) of EQTransformer with five different machine-learning-based pickers, PhaseNet (Zhu and Beroza, 2019), GPD (Ross et al., 2018), PpkNet (Zhu et al., 2019), Yews (Zhou et al., 2019), and PickNet (Pardo et al., 2019). Mean (μ) and standard deviation (σ) of each error distribution and the precision (Pr), recall (Re), F1-score (F1), mean average error (MAE), and the mean average percentage error (MAPE) are given in each subplot.*

The multi-task architecture (Figure 3) has a common input, and is designed for both event detection and phase picking while exploiting the dependency of these detection and phase measurement tasks on each other through a hierarchical structure. With 56 layers, it was the deepest neural network for seismic signal processing at the time of publication. This is significant because, when properly trained, deep networks have greater discriminatory power. We trained it using the global STEAD dataset (*Mousavi et al.,* 2019b), which is described below. EQTransformer uses both local and global attention mechanisms to help make connections between different parts of the seismic time series that are important to the tasks of interest. It was the first, or among the first, attentive models for earthquake signal processing.

We found that EqTransformer outperformed the existing deep-learning and traditional phase-picking and detection algorithms such that it represented the state-of-the-art at the time of publication (Figs. 4-5). The primary gain in performance is achieved for cases with high background noise and for the challenging task of picking the S wave arrival.

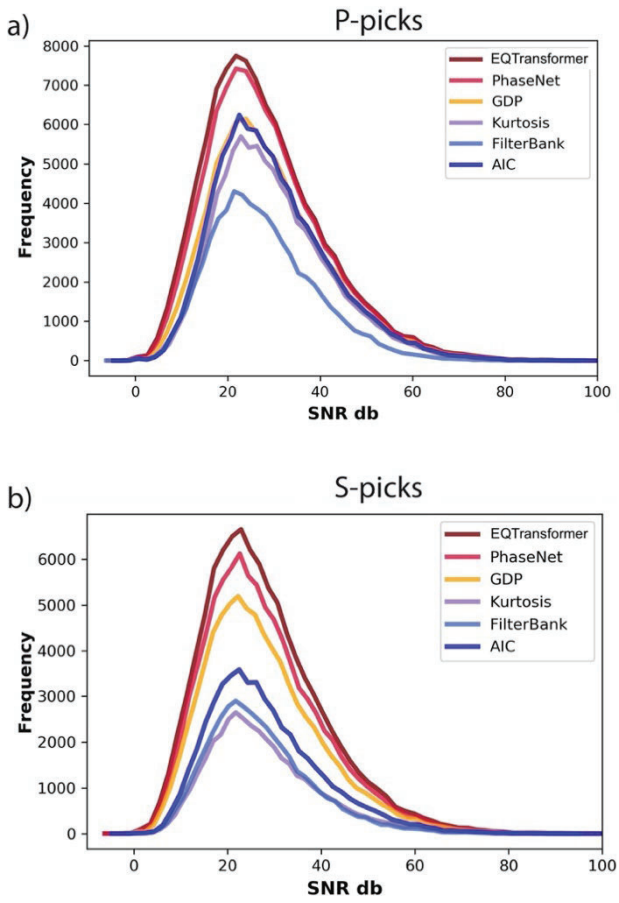

Figure 5. **Comparison of the sensitivity of P (a) and S (b) phase picks as a function of signal-to-noise ratio (SNR) for three deep-learning-based and three traditional phase pickers**. *At the time it was published, EQTransformer outperformed all of the other algorithms across the full spectrum of signal-to-noise ratio (SNR).*

3.2 Benchmark Data Sets for Machine Learning Analysis

Seismology benefits from decades of work by expert analysts in assigning "labels" to seismic waveform data. These labels are immensely valuable and form the essential foundation for much of the progress documented in this report. Supervised machine learning – particularly deep learning – is a data hungry enterprise and known examples or labeled data sets are the essential requisite for building effective supervised models. Seismology has labeled data, but the reliability of those labels is highly variable, and the lack of high-quality labeled data sets to serve as ground truth as well as the lack of standard benchmarks can act inhibit progress. We have sought to accelerate progress by developing standardized quality controlled labelled data sets for developing machine learning capabilities for seismic monitoring applications.

3.2.1 STEAD: The Stanford Earthquake Database. We published a high-quality, large-scale, and global data set of local earthquake and non-earthquake signals recorded by seismic instruments (Fig. 6). The data set contains two categories: (1) local earthquake waveforms (recorded at source-receiver distances of less than 350 km) and (2) seismic noise waveforms that are free of earthquake signals. These data comprise ~ 1.2 million time series or more than 19,000 hours of seismic signal recordings (Fig. 6). We published this data set as STEAD (STanford EArthquake Database) [*Mousavi et al.,* 2019b], and

make STEAD openly available to the community through a GitHub portal at: https://github.com/smousavi05/STEAD. Waveforms are stored in a single 83 Gbyte hdf5 file at https://rebrand.ly/whole, but are also available in 13.7 Gbyte chunks that can be merged after download.

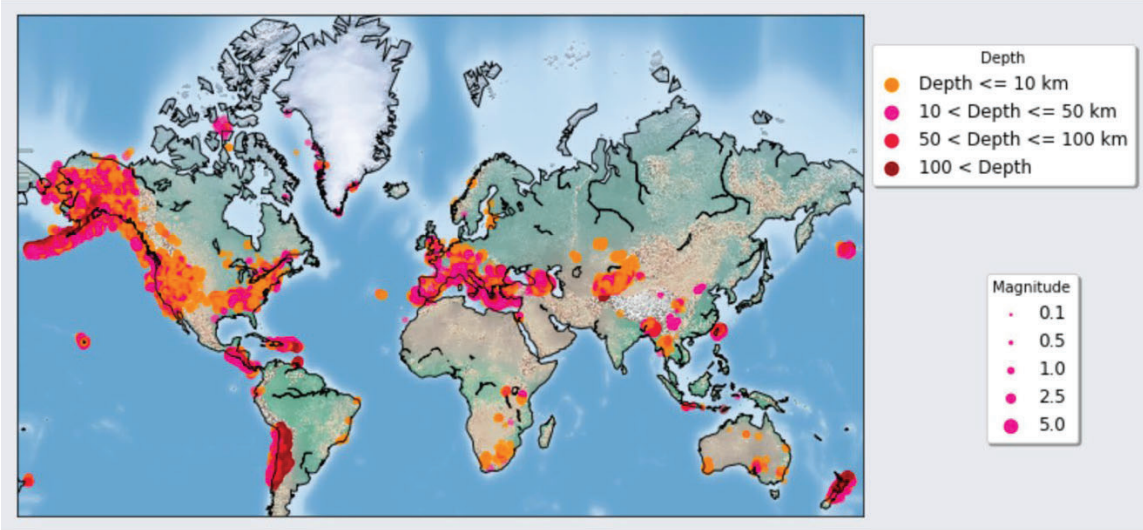

Figure 6. **Location, size, and depth distributions of earthquakes used in STEAD.**

The metadata used in the construction of STEAD included information about the recording stations, recorded earthquakes, and hand-picked parameters, such as arrival times of *P* and *S* waves at each station (Fig. 7). We acquired metadata from multiple sources including: 1) the International Seismological Center, 2) the National Earthquake Information Center, 3) the Northern California Seismic Network, 4) the Southern California Seismic Network, 5) the Pacific Northwest Seismic Network, 6) the New Madrid Seismic Network, 7) the Incorporated Research Institutions for Seismology (IRIS), 8) the Advanced National Seismic System Composite Catalog, 9) the Global Seismograph Network (GSN) and 10) the broader literature. We processed more than 120 million data entries from these resources to extract and re-organize the metadata associated with local waveforms. For the lower magnitude ranges, for which fewer manual picks were available, we used theoretical arrival times. This information was combined with the earthquake and station information to build a comprehensive relational database.

Figure 7. **Sample earthquake seismograms and labels from the database.** *a) The time-series of ground motion for east-west, north-south, and vertical directions respectively. b) The header information (labels) associated with the seismogram. The unit of each label is given in the label name. In compiling STEAD we systematically checked the reliability of existing labels taken from earthquake catalogs and added many new labels of our own. Such labels are essential for training machine learning algorithms and while seismology is fortunate to have large, labelled data sets, it's essential that those labels be accurate.*

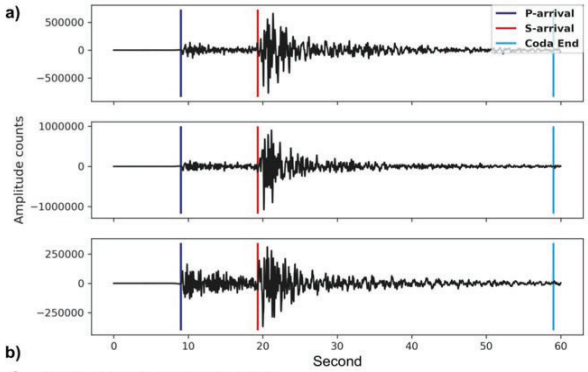


```
{ 'back_azimuth_deg': 222.89999,
'coda_end_sample': 5900.0,
'network_code': 'TA',
'p_arrival_sample': 900.0,
'p_status': 'manual',
'p_travel_sec': 14.99,
'p_weight': 0.5,
'receiver_code': '109C',
'receiver_elevation_m': 150.0,
'receiver_latitude': 32.8889,
'receiver_longitude': -117.1051,
'receiver_type': 'BH',
's_arrival_sample': 1932.0,
's_status': 'manual',
's_weight': 0.5,
'snr_db': array([ 56. ,  58.1,  55.4]),
'source_depth_km': 10.21,
'source_depth_uncertainty_km': None,
'source_distance_deg': 0.81,
'source_distance_km': 89.669998,
'source_error_sec': 1.3719,
'source_gap_deg': 31.705999,
'source_horizontal_uncertainty_km': 3.2019601,
'source_id': '602597568',
'source_latitude': 33.4826,
'source_longitude': -116.4524,
'source_magnitude': 4.7,
'source_magnitude_author': None,
'source_magnitude_type': 'mb',
'source_mechanism_strike_dip_rake': array([[ 216.48,   71.12,   -6.16],
   [ 308.48,   84.17, -161.02]]),
'source_origin_time': '2013-03-11 16:56:05.86',
'source_origin_uncertainty_sec': 0.69,
'trace_category': 'earthquake_local',
'trace_name': '109C.TA_20130311165610_EV',
'trace_start_time': '2013-03-11 16:56:11.850000'}
```


In addition to the size of the labeled data set, the accuracy of the labels is important to developing effective models. In constructing STEAD, we carried out extensive quality control to minimize four kinds of errors known to be present in the waveform data:

1) earthquake characterization errors: these include errors in location, depth, origin time, and magnitude estimates of the earthquakes and can be due to errors in the arrival time picking, inaccurate velocity models, non-robust algorithms, number of recording stations, etc. These errors can also affect the calculated epicenter distance, back azimuth, and P travel time.
2) errors in arrival time picks: these are either due to inaccurate theoretical arrival time estimates or human errors in the manual picks.
3) Missing signals: Some time series do not contain the expected earthquake signals. This could be due to either inaccurate theoretical arrival time estimation during the preparation of the database or to timing errors between phase catalogs and archived data.
4) Multiple events: Some time-series contain multiple uncatalogued, and thus unlabelled, earthquakes in addition to the known earthquakes as described above. Prior to compiling STEAD, we did not appreciate how common this was.

We randomly selected one-minute noise waveforms from the time periods between the cataloged earthquakes. After performing the same pre-processing (detrending, band-pass filtering, and resampling), we performed post-processing consisting of de-signaling followed by double checking using the generalized earthquake detector, CRED to ensure that the noise traces do not contain earthquake signal (even hidden within the background noise). The de-signaling algorithm used here is a combination of the methods introduced in Mousavi and Langston (2016) and Mousavi and Langston (2017) that identifies the anomalous spectral features associated with earthquake signals (based on statistical considerations) in a continuous wavelet domain.

STEAD is an open-access, high-quality, large-scale global labeled data set of earthquake and non-earthquake signals recorded by seismic instruments. Benchmark data sets such as STEAD can accelerate progress in applying machine learning to problems in seismology by facilitating validation and comparison of competing methods, which promotes adoption of best practices and accelerates research progress.

At the time of its publication, the scale and the accuracy of STEAD presented novel opportunities to researchers in the seismological community and beyond. STEAD included introductory material on seismic monitoring in an attempt to recruit interest from data science expertise beyond seismology. STEAD seems to have inspired parallel efforts including the creation of the LENDB (*Magrini*, 2020), INSTANCE (*Michelini et al.,* 2021), MLAAPDE (*Cole et al.*, 2023) and CREW (*Aguilar and Beroza*, 2023) datasets. Others have responded by creating QuakeLabeler, which is a Python package developed by *Mao and* Audet that enables the development of ground truth labels and conversion of new data into STEAD format. Also related and very useful is the seismological data science ecosystem SeisBench (*Woollam et al.,* 2022), which is an open-source python toolbox for machine learning in seismology. Seisbench provides a unified API for accessing, training, and applying machine learning algorithms to seismic data, and is available at: https://github.com/seisbench/seisbench.

3.2.2 CREW: Curated Regional Earthquake Waveform Database. We have developed a regional seismic phase database CREW (Curated Regional Earthquake Waveforms) and submitted it for publication to the diamond open access journal *Seismica (Aguilar and Beroza*, 2023). Figure 8 illustrates the contrast in the characteristics of direct crustal arrivals Pg and Sg at local distances, and *Pn* and *Sn* and regional distances for the 2023 Lake Almanor, California earthquake. The example shown at ~500 km distance is beyond the crossover distance at which *Pn* and *Sn* are the first arriving P and S phases, and these phases are relatively weak and emergent. CREW is meant to provide for regionally recorded *P* and *S* phases what STEAD provides for locally recorded seismic phases, *viz.* a large waveform database with extensive and accurate labels for developing and testing machine learning models.

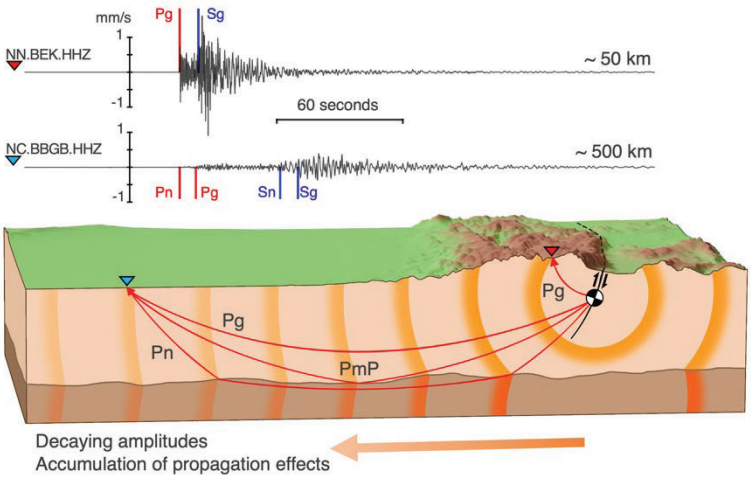

Figure 8. **Comparison of local and regional recordings for the 2023 Lake Almanor earthquake in Northern California.** *The top waveform was recorded at ~ 50 km while the bottom one was recorded at about 500 km. (after Aguilar and Beroza, 2023).*

Figure 9 illustrates the importance of regional phases for seismic monitoring. For most of the world – even in seismically active regions – regional phases are required for monitoring. This is strong motivation to develop machine learning models that optimize performance for regional seismic phases. For the oceans, as well as large swaths of Africa and North-Central Russia, there is not regional coverage, so only teleseismic monitoring is available. Figures 10 and 11 illustrate the distribution of data in CREW.

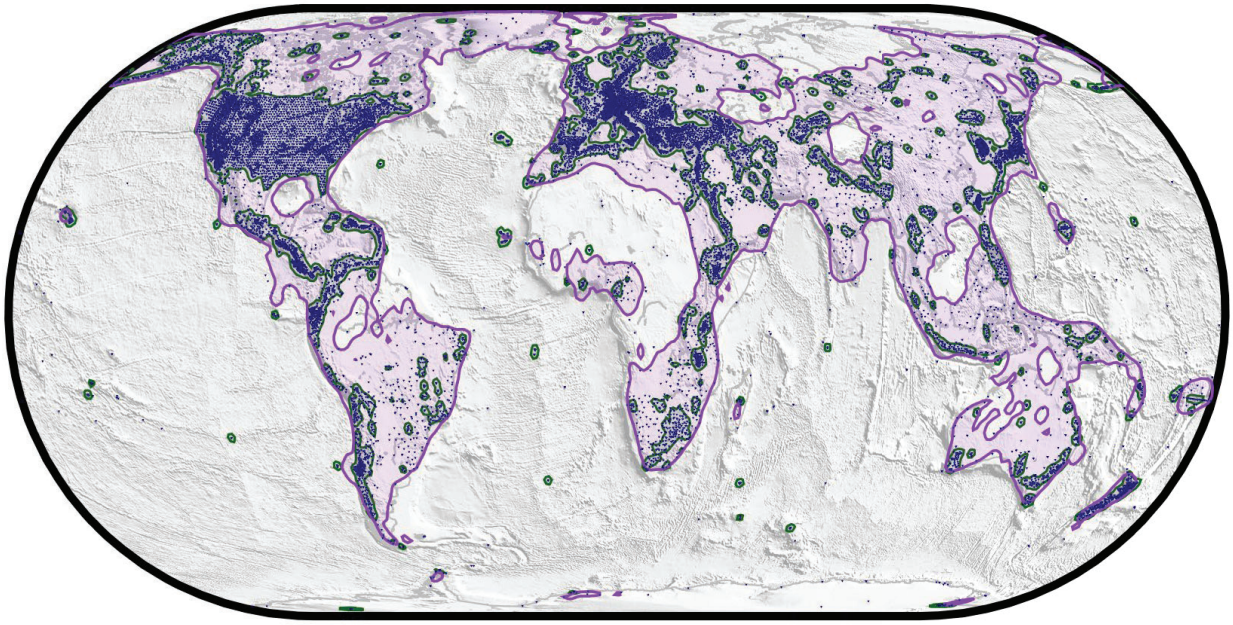

Figure 9. **Stations in the ISC inventory list.** *Green regions are those for which there are at least 5 stations within a 3 degree radius and the purple regions are those for which there are a minimum of 5 stations within a 10 degree radius and the azimuthal gap for an earthquake within this region would be less than 180 degrees. Note that coverage is not as complete as noted here because this map includes coverage from temporary (i.e., PASSCAL and Transportable Array) stations. (after Aguilar and Beroza, 2023).*

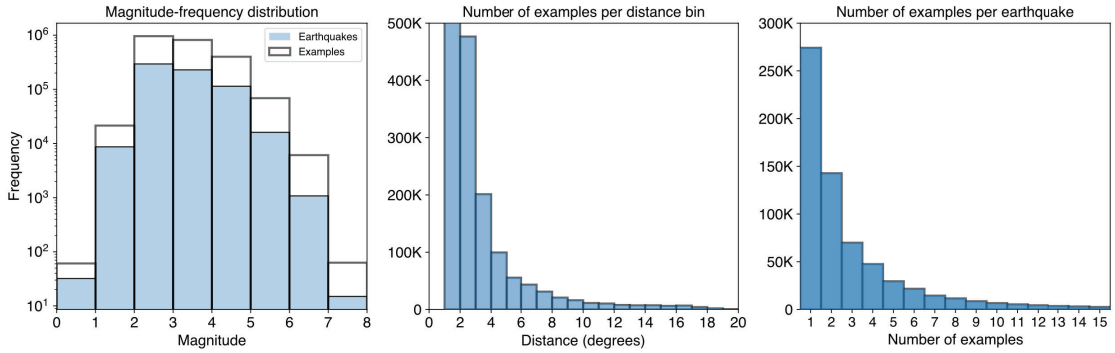

Figure 10. **Magnitude-Frequency distribution**. *Solid bars display the distribution of unique earthquakes in the dataset. The empty bars display the frequency distribution if each example is treated as a separate magnitude. Middle. Distribution of source to receiver distances, which span 1 to 20 degrees. Right. Number of waveforms of examples in the dataset per each unique origin ID, for most earthquakes there are only one or two observations, whereas examples having more than 5 is rather scarce in the database. (after Aguilar and Beroza, 2023).*

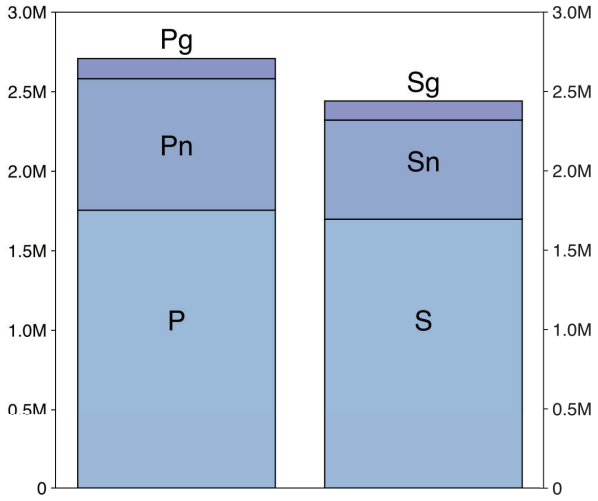

Figure 11. **Number of picks in CREW for each category.** *The phases labeled P and S are undifferentiated arrivals of that wavetype. (after Aguilar and Beroza, 2023)*

3.3 Machine Learning for Earthquake Characterization

Characterization, which refers to the estimation of source characteristics such as magnitude, focal mechanism, and stress drop to known earthquakes often represents the final task in developing an earthquake catalog. Here too, we can demonstrate the power of machine learning methods to improve upon standard practice.

3.3.1 MagNet: A Machine Learning Model for Magnitude Determination. Earthquake magnitude is a fundamental parameter that represents the strength of a seismic source. It is usually determined from the amplitude and sometimes – explicitly or not – the period of a specified seismic wave using a formula that contains several constants. These constants are

determined in such a way that the magnitudes are independent of where an event was recorded (i.e., distance) and such that different magnitude scales agree with one another to the extent possible. Most methods for determining magnitude require several steps. For the local magnitude, M_L these include: 1) remove the instrument response, 2) convolve the seismogram with the response of a Wood Anderson instrument, 3) convert the raw seismograms into displacement, 4) if attenuation and site correction terms are known for the region, estimate magnitudes at each station, and 5) average the single-station estimates to average over source, site, and path effects. Our goal was to develop an alternative method for a fast and reliable estimation of earthquake magnitude directly from raw seismograms recorded on a single station using machine learning.

A challenge to this ambition is that amplitude information plays a key role in magnitude determination, but the training of typical neural networks depends on data normalization, which negates amplitude information. For this reason, we designed a network of convolutional and recurrent layers that we call "MagNet" where the convolutional layers do not have any activation function but are used only for dimensionality reduction and feature extraction (Figure 12).

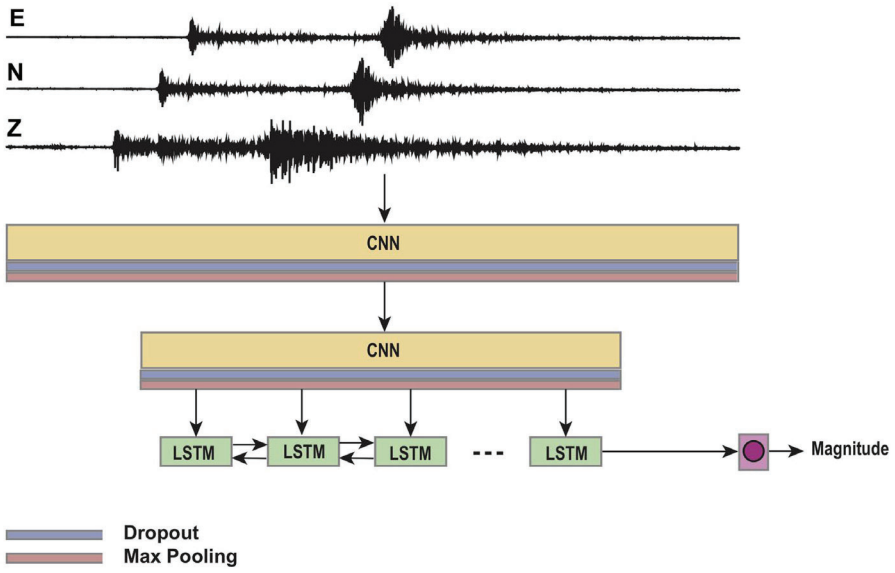

Figure 12. **Network architecture of MagNet consisting of two (CNN) and one bidirectional long-short-term-memory (LSTM) layers**. *Layers do not have activation functions, and each is followed by a dropout and maxpooling layer.*

MagNet results are presented in (Figure 13). The results show a mean error close to zero and standard deviation of ~0.2. The regression performance is worse at upper and lower bounds where fewer training/test samples are available for larger and smaller magnitudes respectively. The network can predict both local and duration magnitudes with reasonable accuracy, which indicates its ability to learn both attenuation and duration, directly from the input waveform from a single station.

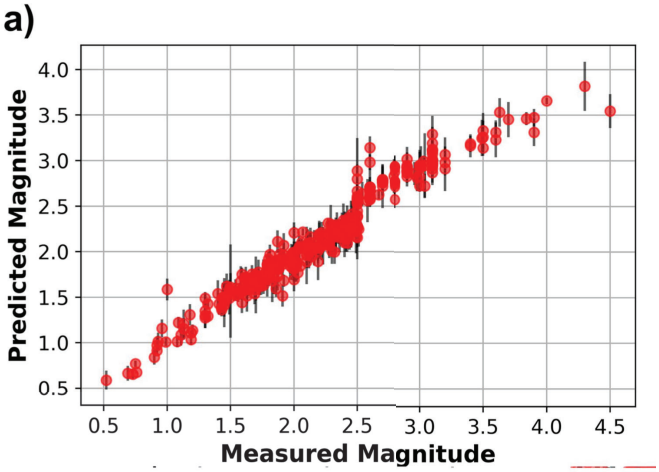

Figure 13. MagNet single-station magnitude **predictions vs. traditionally measured magnitude.** *The correlation is strong, except at larger magnitudes where data are relatively sparse.*

We note that we only tested this on earthquakes of magnitudes ~4 and smaller that were locally recorded (we used STEAD), so there remains much work that could be done to improve the method, apply it at larger distances, and test it on a wider spectrum of earthquakes. The paper describing MagNet is published in *Geophysical Research Letters* (*Mousavi et al.,* 2020a), and the package is available for download at: https://github.com/smousavi05/MagNet.

3.3.2 A Machine Learning Model for Single-Station Location. We developed a deep-learning method for earthquake location using waveforms from a single-station. We approach location as a regression problem using two separate Bayesian neural networks (*Mousavi and Beroza,* 2020b).

The first model is a multitask temporal convolutional neural network (TCN) to learn epicentral distance and P travel time from 1-minute seismograms of local earthquakes. We designed a separate multi-input network using standard convolutional layers to estimate the back-azimuth angle and its epistemic uncertainty. We used the output of these machine learning models to estimate the epicenter, origin time, and depth along with their confidence intervals.

We trained these networks on a global data set of earthquake signals recorded within 1° (~111 km) from the event to build the model and demonstrate its performance. Fig. 14 shows regression results for the test set. The network can estimate *P*-wave travel time with a standard deviation of 0.66 s. The mean error for epicentral distance estimates is 0.23 km with a standard deviation of 5.42 km. Compared with these results, back-azimuth estimates are more uncertain. This is mainly due to the complication of estimating orientation; however, a coefficient of determination of 0.87 for the regression results and a mean error rate of ~1°, which is impressive given that only 1.5 s of the waveforms are used for those estimates. Fig. 15 compares examples of our inferred locations, with error estimates, with results from local/ regional seismic network catalogs. This approach can be used for fast source characterization with a limited number of observations or for estimating the location of earthquakes that are sparsely recorded—either because they are small or because stations are widely separated.

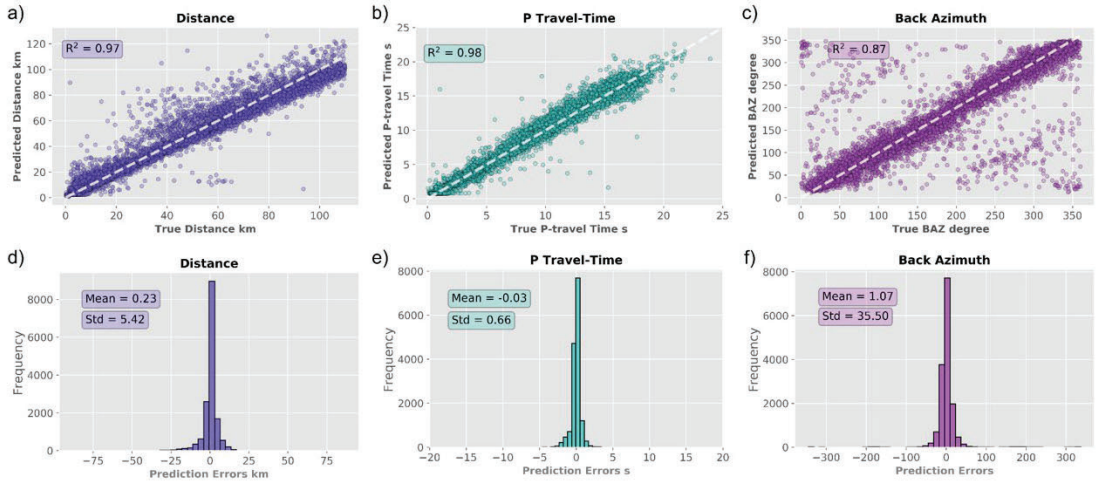

Figure 14. **Regression results for (a) Epicentral distance, (b) P travel-time, and (c) Back-azimuth angle estimations are provided in the upper row. Histograms depicting (d) Distributions of errors for distance, (e) P travel-time, and (f) Back azimuth are presented in the lower row.**

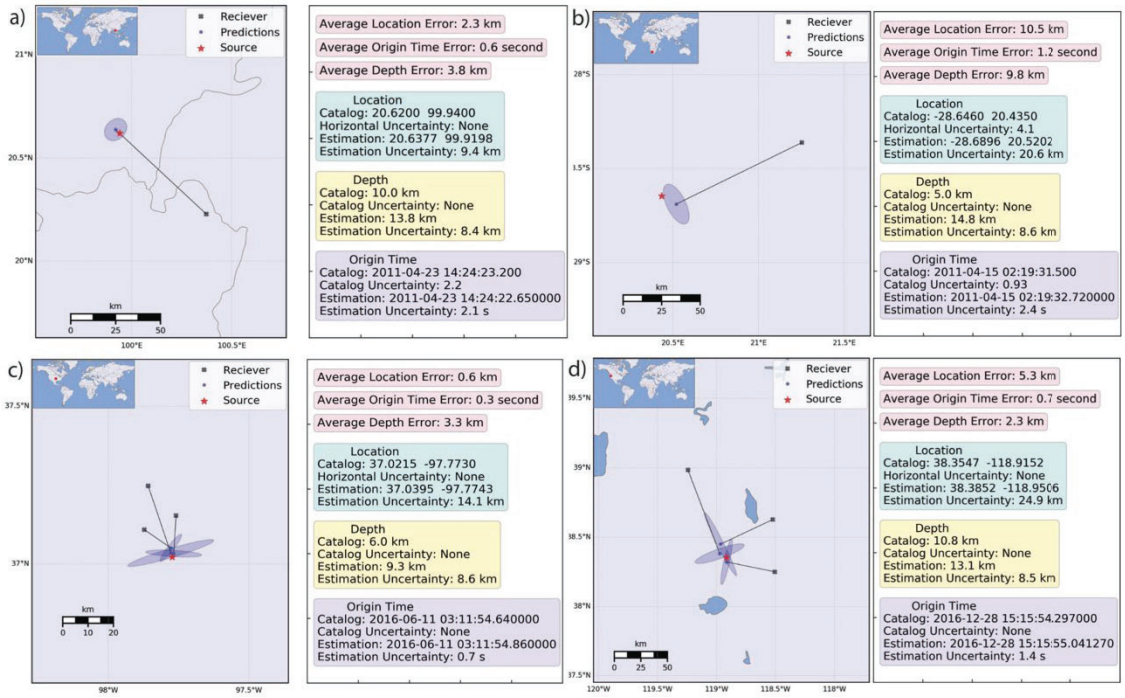

Figure 15. **Four examples of single-station location estimates and associated error based on predicted back-azimuth and epicentral distance.** *For each event, we estimate errors based on averaged results (without weighting) for multiple observations. (a) ML 1.7 earthquake in Myanmar. (b) ML 1.6 in South Africa. (c) ML 2.1 in Southern Kansas. (d) ML 2.3 south of Reno, Nevada, respectively. See Mousavi and Beroza (2020b) for more examples.*

3.4 QuakeFlow: A Cloud-Based Machine-Learning Workflow for Seismic Monitoring

Earthquake monitoring workflows are designed to detect earthquake signals and to determine source characteristics from continuous waveform data. Deep learning has been used to improve tasks within earthquake monitoring workflows to allow fast and accurate detection of up to orders of magnitude more small events than are present in conventional catalogues. Applying these machine learning methods to revisit archived seismic data sets is rewarding, but computationally challenging. We developed a cloud-based earthquake monitoring workflow, QuakeFlow, which applies multiple processing steps to generate earthquake catalogs from raw seismic data (Figure 16) at scale. QuakeFlow uses a deep learning model, PhaseNet (*Zhu et al.,* 2019), for picking P/S phases and a soft clustering method, GaMMA (*Zhu et al.,* 2022), for phase association with approximate earthquake location and magnitude. Each component in QuakeFlow is containerized, Containerization such that the code is bundled with the files/libraries required to run on in any environment, which facilitates: updates to the pipeline with new deep learning/machine learning models, comparison across competing methods, and the ability to add new algorithms.

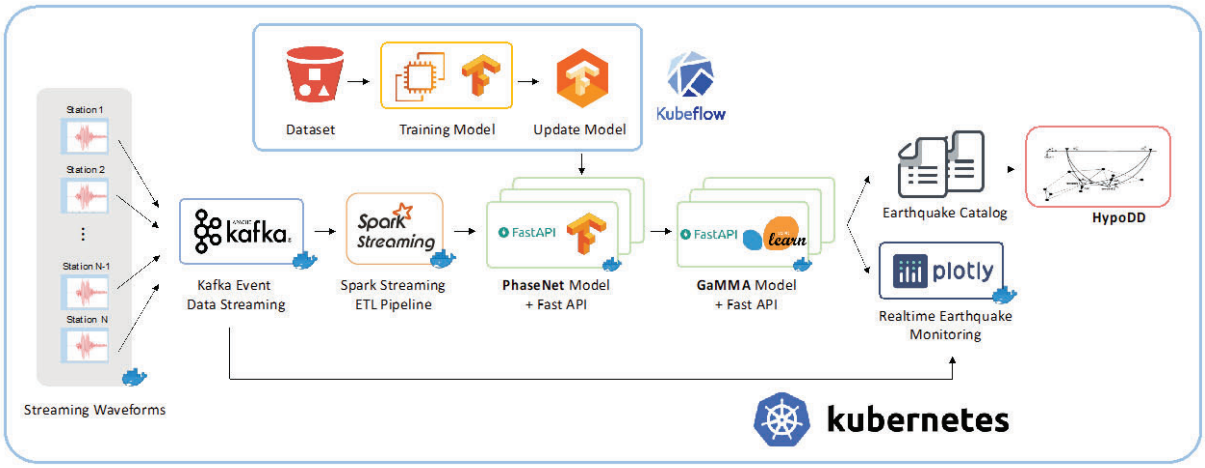

Figure 16. **The workflow of Quakeflow**. *We have tested it both on large data archives and for real time processing with streamed data.*

3.4.1 Data Streaming. Apache Kafka is a fault-tolerant, highly scalable, distributed messaging system for streaming applications (*Kreps et al.* 2011). In QuakeFlow, Kafka acts as the central hub for real-time streaming of waveform data and model prediction results. We use three pre-defined Kafka topics: (1) "waveform raw," (2) "phasenet picks," and (3) "gamma events," to organize, send, and receive data. The monitoring stations continuously send fragments of seismic waveforms to topic waveform raw. We then use the scalable, fault-tolerant Spark Streaming processing system, which is an extension of the core Spark API that supports both batch and streaming workloads (*Zaharia et al.* 2013), as an extract-transform-load (ETL) pipeline to apply data transformations and pre-processing to the streaming data. Spark Streaming supports operations to aggregate streaming data over a sliding window. We group the streaming data in a specified window size (e.g. 30 s) using a sequence of MapReduce operations to prepare a structured data

format for subsequent processing of PhaseNet and GaMMA. The outputs of these machine learning models are broadcast to the phasenet picks and gamma events topics, respectively. Finally, the earthquake detection results can be saved and visualized by subscribing to the corresponding Kafka topics.

3.4.2 Autoscaling. We deployed QuakeFlow in Kubernetes, which is an open-source system for automating deployment, scaling, and management of containerized applications, to make it cloud-platform-independent and applicable to both on-site servers and any cloud-platforms with Kubernetes services. Kubernetes automatically orchestrates different components of QuakeFlow to make it run on the cloud efficiently. We used horizontal pod auto-scaling provided by Kubernetes, and the node auto-provision provided by cloud-platforms, such as Google Cloud Platform (GCP), to match computational resources automatically with computational load. We carried out a simple pressure test on GCP using a maximum of eight computational nodes of machine type 'n2-standard-2'11 (2 vCPU and 8GB of memory) to evaluate the speedup using auto-scaling when processing a large data volume. Figure 17(a) shows that the computational time with auto-scaling is significantly reduced compared to the computational time without it. Data throughput, that is the number of waveform-hours processed per second, linearly increases with the data volume when auto-scaling is enabled (Figure 17b). This means that we can apply auto-scaling for embarrassingly parallel large-scale seismic data mining.

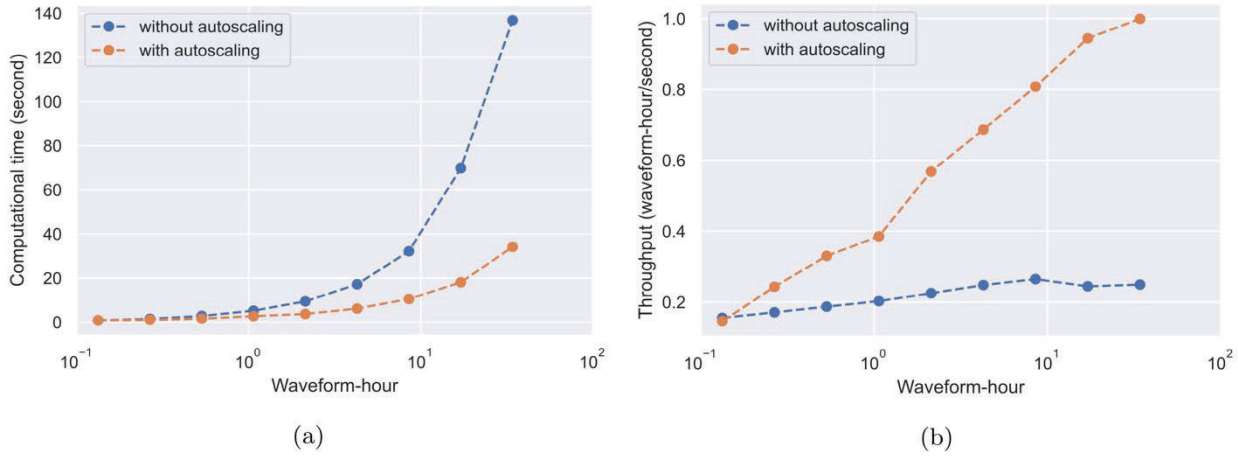

Figure 17. **Computational advantages of auto-scaling: (a) computational time; (b) data throughput. (after Zhu et al., 2023).**

4. RESULTS AND DISCUSSION

4.1 EQTransformer Example Application

STEAD, the dataset used for training of EQTransformer, does not include waveform data from Japan, which made that an ideal place to test its performance and ability to generalize to out of distribution data. We select the 2000 Mw 6.6 western Tottori aftershock sequence for our test. We applied our detector/phase-picker model to continuous waveform data from

18 HiNet stations from 6 October to 17 November 2000. We associated phase picks to individual events in origin-time space, used Hypoinverse (*Klein*, 2002), and then HypoDD (*Waldhauser and Ellsworth*, 2000) to locate and relocate the associated events. We used both travel time differences and cross-correlation relative arrival time measurements for relocation.

We detected and located 21,092 events within this time period (Figure 18). This is more than a two-fold increase in the number of events compared to *Fukuyama et al.* (2003) during the same time period using hand-picked phases provided by the Japan Meteorological Agency (JMA). Our catalog includes almost all events reported by JMA despite the fact that we used only a about a third of the stations. JMA's analysts picked 279,104 *P* and *S* arrival times on 57 stations, while EQTransformer picked 401,566 *P* and *S* arrival times on 18 stations (due to unavailability of data for other stations).

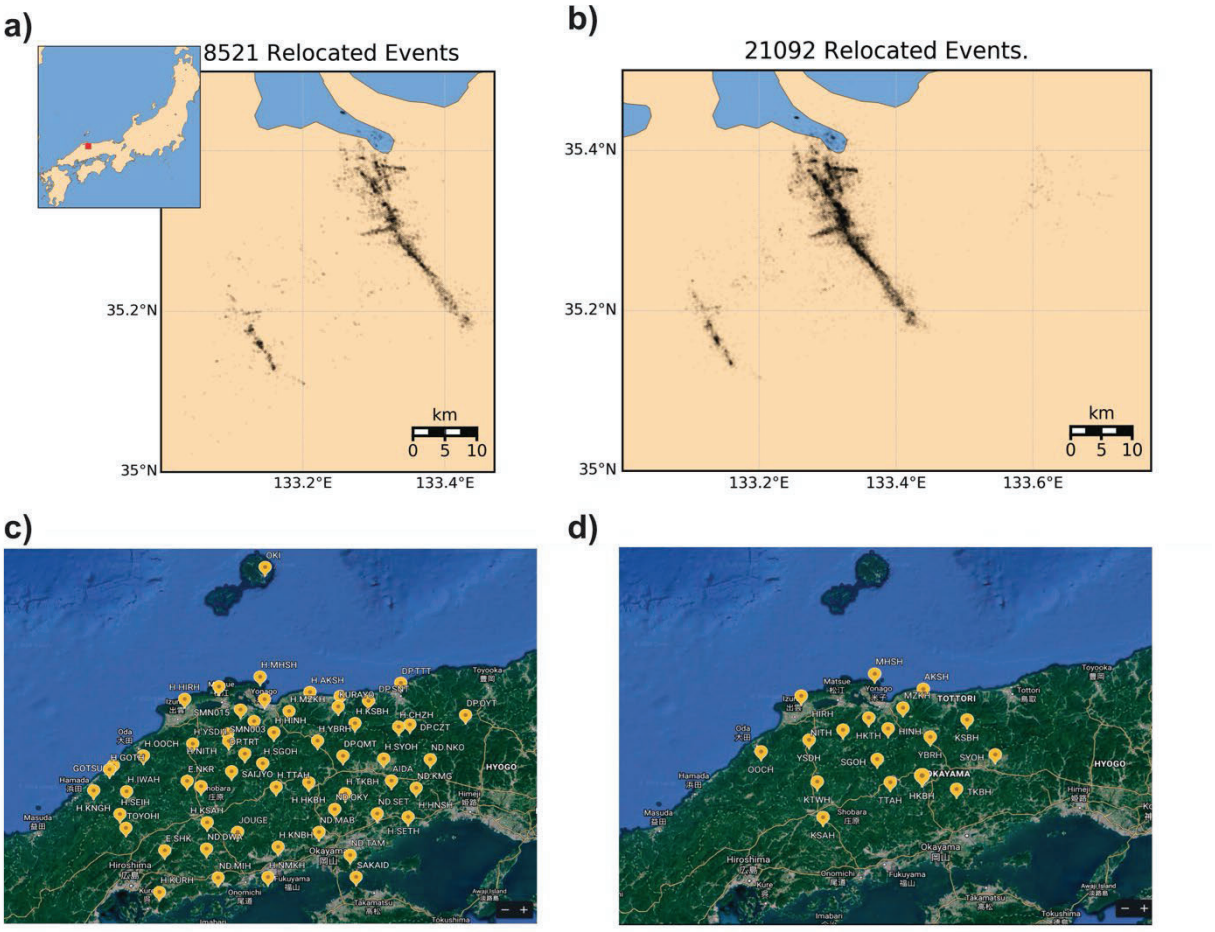

Figure 18. **Seismicity of the Tottori region between 6 October and 17 November 2000**. *a) relocated events using manual phase picks by JMA. b) relocated events using EQTransformer. c) Distribution of 57 seismic stations used by Fukuyama et al. (2003) d) distribution of 18 stations used in our study to detect and locate earthquakes in the Tottori region.*

To compare the manual picks by JMA with our automatic picks we used about 42,000 picks on the common stations and calculated the arrival time differences. The distributions of these arrival time differences between the manual and deep-learning picks for P and S waves are shown in Figure 19. The standard deviation of differences between picks are around 0.08 second with mean absolute error of around 0.06 second or 6 samples. Results are slightly better for S picks. The mean error is 1 sample.

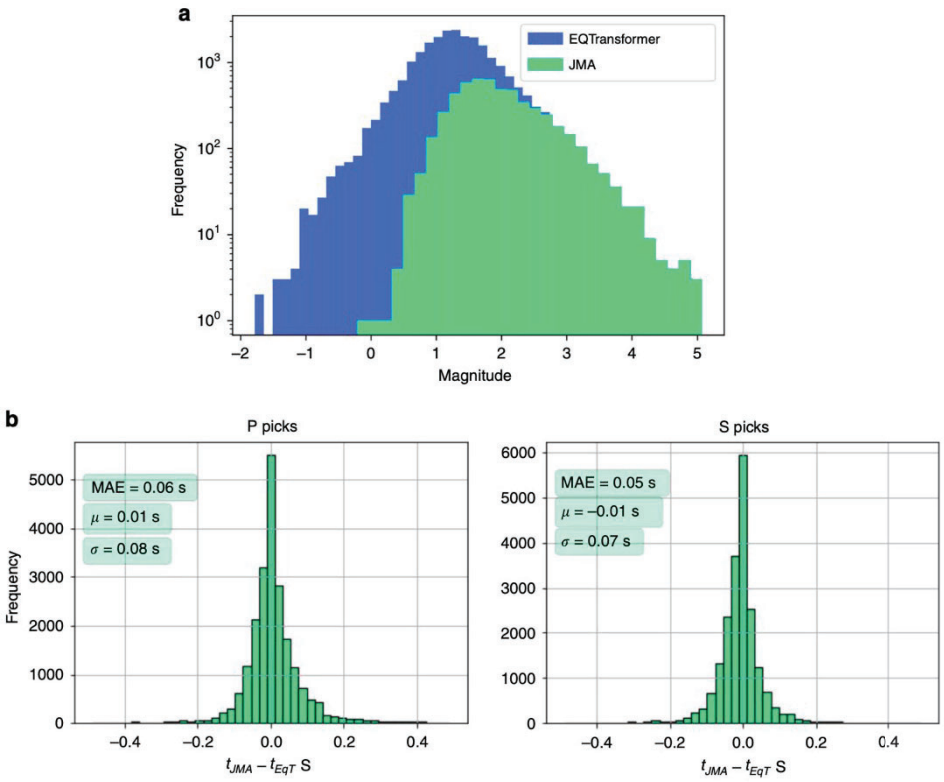

Figure 19. **Distributions of frequency magnitude of earthquakes and picking errors.** *(a) frequency-magnitude distributions of located events in JMA catalog and relocated events in our catalog (EQTransformer). Magnitudes for all events have been estimated using a local magnitude scale. (b) distributions of arrival-time differences (in seconds) between P (left) and S (right) picks by JMA's analysts and EQTransformer.*

4.2 Quakeflow Example Applications

We used QuakeFlow to process three years of continuous archived data from Puerto Rico. The earthquake sequence in Puerto Rico started on December 28, 2019 and continued through 2021. The largest earthquake (*M* 6.4) to date occurred on 2020 January 7, causing many injuries and widespread damage (*Vanacore et al.,* 2022). The sequence was rich in seismicity and involved both strike-slip and normal faulting (*ten Brink et al.* 2022). Deformation in this area is transtensional and diffuse, with unmapped faults capable of generating moderate-to-large earthquakes (*Viltres et al.* 2022).

We tested QuakeFlow's detection performance and processing speed by applying it to three years of archived data from 2018-05-01 to 2021-05-01 using 70 stations within a region 65° W–68° W and 17° N–19° N (Figure 20a) for approximately 210 station-years of three-component continuous data from the Puerto Rico Seismic Network (University of Puerto Rico 1986) and the US Geological Survey Networks (Albuquerque Seismological Laboratory (ASL)/USGS 1980). We ran QuakeFlow on GCP with auto-scaling using a maximum of 60 computational nodes of machine type 'n2-standard-2' (2 vCPU and 8GB of memory). Downloading waveform data from the IRIS data center using ObsPy took ~ 3.5 hr, depending on internet conditions and data center server load. Picking P and S phases using PhaseNet took ~ 3 hr, and associating phases using GaMMA took ~ 30 min. The entire process was fast enough to run overnight. Total cost of this processing was around $40 based on a price of $0.07/hour per node. The detection results are shown in Fig. 20 b-d. Compared with the standard catalog generated by the Puerto Rico Seismic Network, QuakeFlow detected over an order of magnitude more small earthquakes, particularly during active aftershock periods. The number of earthquakes depends on hyperparameters, with a trade-off with false positives. Quantification of this trade-off is an important direction for future research.

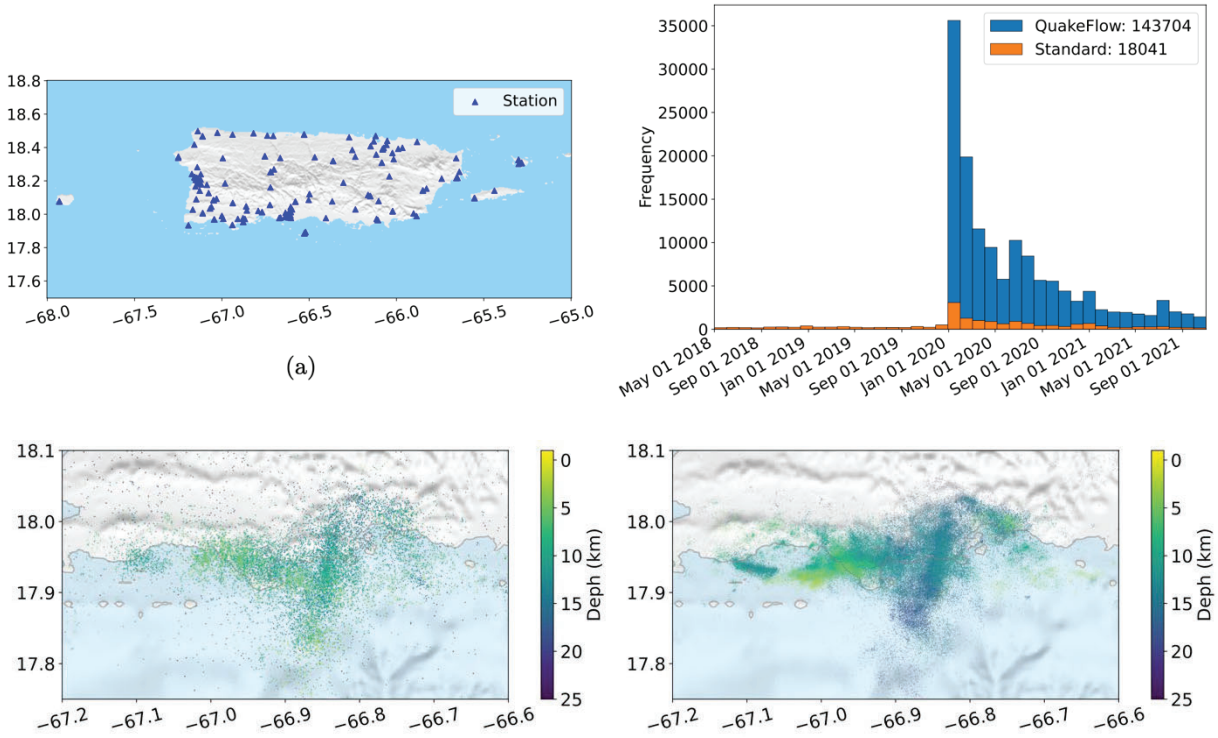

Figure 20. **QuakeFlow results for three years of Puerto Rico data**. *Upper left shows station distribution. Upper right shows time-history of earthquakes. QuakeFlow (lower right) found ~8 times more earthquakes than the standard catalog (lower left). Depths in QuakeFlow are biased due to the simplified assumptions used in association, but it's clear that the same structures are being illuminated in both catalogs, and that the QuakeFlow catalog is more complete. (after Zhu et al., 2023).*

We applied QuakeFlow to study volcanic earthquakes on the big island of Hawaii, which has seen a surge of eruptive activity, including the collapse of Kilauea Caldera (Fig. 21). We experimented with running it on streaming data in near real time, but eventually worked with archived data. For that we retrieved continuous seismic waveforms for 66 stations from the Hawaii Volcano Observatory Network (HVO) (USGS Hawaiian Volcano Observatory (HVO) 1956). With only a few hours of cloud computing, we detect over a factor of 10 more earthquakes than in the standard catalog reported by Hawaii Volcano Observatory Network over the same time period. We find many deep events (below 30 km) in the Pahala Mantle feature that showed a surge of activity since 2015 and is thought to be caused by the emplacement of new magma (*Burgess and Roman,* 2021).

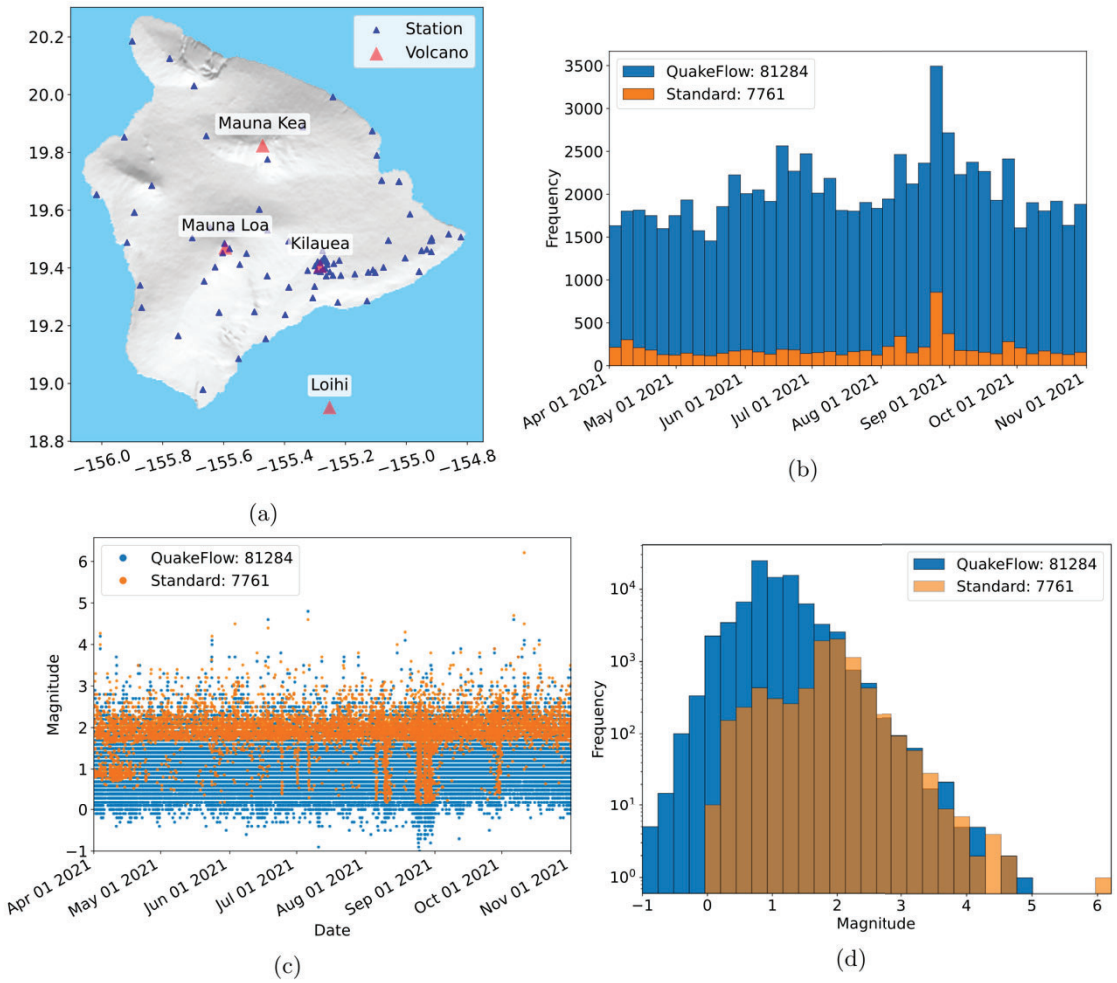

Figure 21. **Statistics for earthquake catalogs in Hawaii.** *(a) seismic station locations; (b) earthquake frequency; (c) earthquake magnitude; (d) earthquake magnitude-frequency distribution. Blue indicates QuakeFlow results. Orange indicates the standard catalog. Unsurprisingly, the newly detected events are all small, with magnitudes ranging from 0 to approximately 2. Note that earthquake magnitudes are approximately estimated during phase association using GaMMA. (after Zhu et al., 2023)*

We have made the QuakeFlow codebase available to the community at: https://github.com/wayneweiqiang/QuakeFlow.

5. REVIEW OF MACHINE LEARNING IN EARTHQUAKE SEISMOLOGY

We responded to an invitation from *Annual Reviews of Earth and Planetary Sciences* to contribute a review of machine learning in Seismology (*Mousavi and Beroza*, 2023). It includes a meta-analysis of trends in seismological applications of machine learning. Among the trends we discerned are an unexpected decrease in the rate of publication of new machine learning models (Figure 22) – note that this is for machine learning *models* not for machine learning *applications*, for which the number of papers is no doubt growing rapidly. That paper also documents strong variations in machine learning approach depending on the task being undertaken (Figure 23).

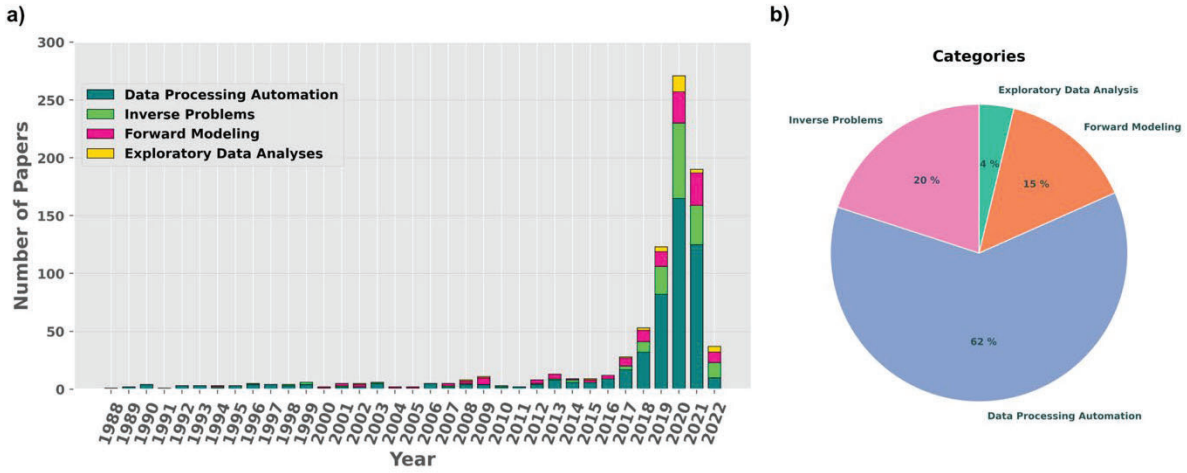

Figure 22. **Publication trends in seismological machine learning**. *a) number of publications applying ML to a seismological task as published between January 1988 and May 2022. Bars are color coded based on task category. b) pie chart showing share of seismological tasks for ML applications. (after Mousavi and Beroza, 2023)*

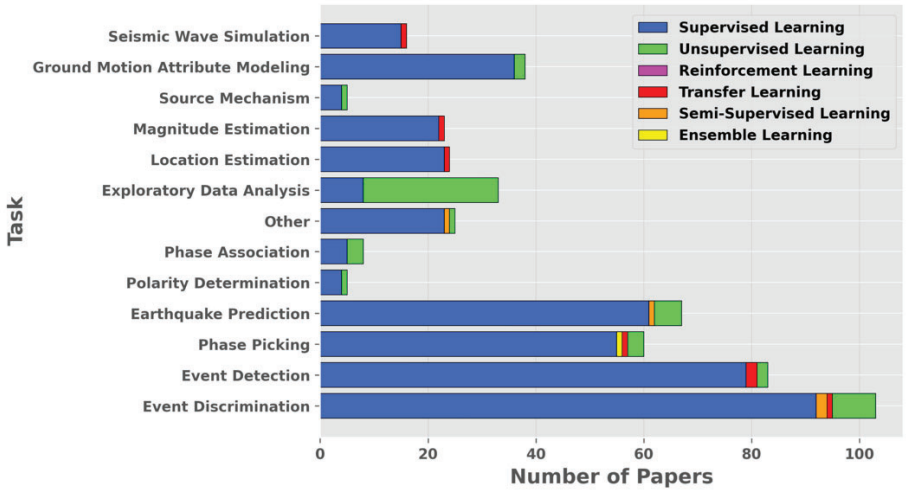

Figure 23. **Distribution of different approaches for different seismological tasks**. *There is a strong variation based on the task. Most effort has been expended in supervised methods, but unsupervised methods are gaining in popularity. Reinforcement, ensemble, transfer, and semi-supervised learning have seen only sparse application. (after Mousavi and Beroza, 2023)*

6. REVIEW OF DEEP LEARNING SEISMOLOGY

When writing the review paper for *Annual Reviews of Earth and Planetary Sciences,* we had more material than could fit in their format. We approached Science about their interest in a review of deep learning in seismology. They agreed to consider it, and we developed a systematic overview of deep-learning in seismology through a meta-analysis of 637 journal papers published between January 1988 and January 2022 (Mousavi and Beroza, 2022). a meta-analysis of 637 journal papers published between January 1988 and January 2022 (*Mousavi and Beroza,* 2022*)*. Unlike the other review, the organization of this review was on all aspects of seismology in which neural networks with many hidden layers have been applied. Deep learning has entered almost every subfield of seismology, and has shown the ability to outperform classical approaches, often dramatically, for tasks such as denoising, earthquake detection, phase picking, seismic image processing and interpretation, and inverse and forward modeling. Some properties of deep neural networks – such as their universal approximation capability, automatic feature extraction, and dimensionality reduction – have been shown to be particularly advantageous in processing complex and high-dimensional waveform data, which often are noisy and incomplete (Fig. 24). Deep learning may be particularly effective for seismological problems for which the underlying physical processes are incompletely understood but for which the data are abundant and of high quality. Fig. 25 illustrates the size and type (synthetic vs. observed) of data sets used to train deep learning models, as well as the number of papers devoted to each task. Among the data-driven tasks, phase picking, event detection, and event discrimination, which are critical to the AFRL program, all stand out. The paper concluded with some speculation on future trends and with recommendations to accelerate progress.

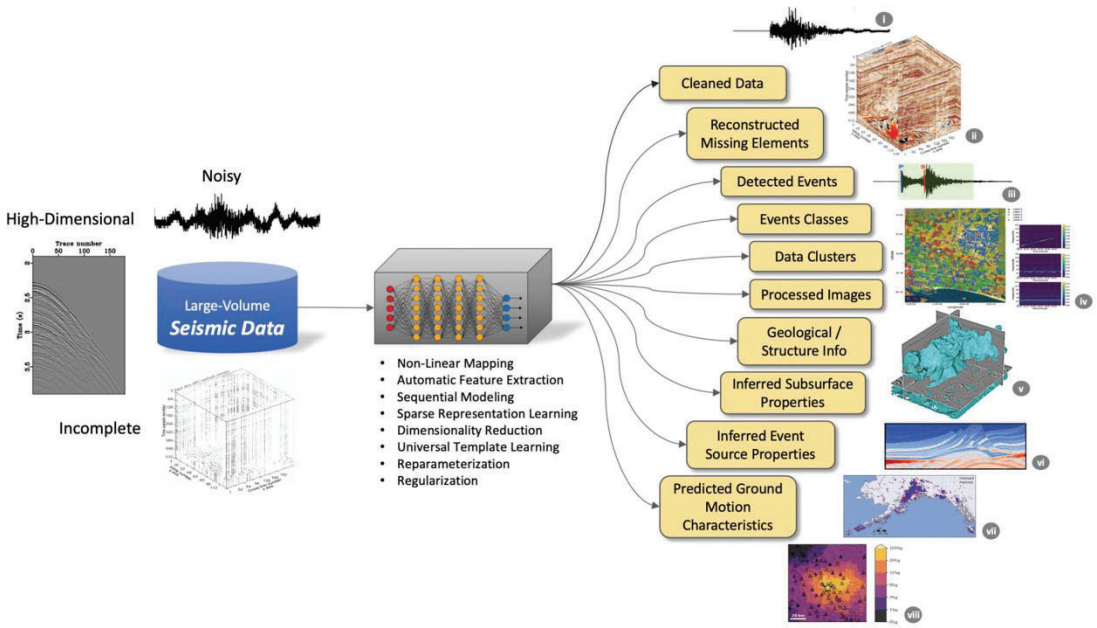

Figure 24. **Properties of deep neural networks, such as their universal approximation capability, automatic feature extraction, and dimensionality reduction are advantageous for processing large, complex seismic recordings, which are noisy and incomplete**. *These are used to build models for seismological tasks. (after Mousavi and Beroza, 2022)*

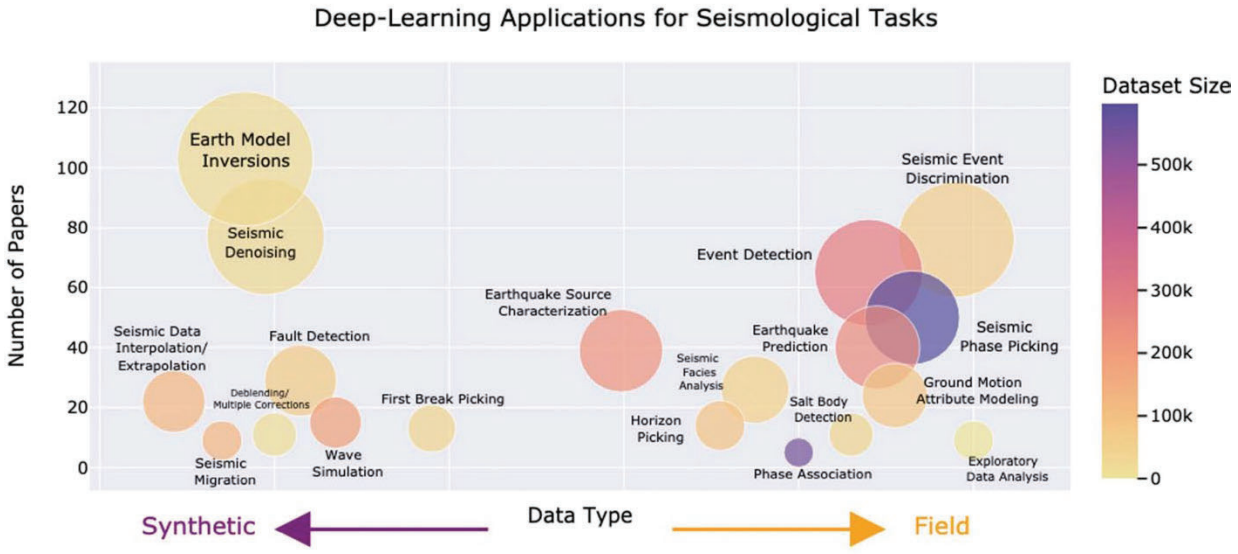

Figure 25. **Deep-learning applications for seismological tasks.** *The size of each circle is scaled with the number of published papers for each application and color-coded according to the average size of training data. Horizontal axes represent the average percentage of observational and recorded data versus synthetic training data. (after Mousavi and Beroza, 2022)*

7. CONCLUSIONS

The goal of this project was to advance machine learning methods for earthquake detection in particular and for seismic monitoring in general. We have achieved that through the creation of benchmark data sets for training machine learning models at local (*Mousavi et al.,* 2019b) and regional (*Aguilar and Beroza*, 2023) distances. For seismic event detection we developed initially the convolutional-recurrent CRED model (*Mousavi et al.*, 2019) and subsequently the multi-task, attentive EQTransformer model (*Mousavi et al.,* 2020). We also developed the MagNet machine learning model (*Mousavi and Beroza*, 2020a) for earthquake magnitude determination and a pair of machine learning models (*Mousavi and Beroza*, 2020b) for seismic event location using a single station. Finally, we developed QuakeFlow (*Zhu et al.,* 2023) to combine the impressive earthquake detection performance of machine learning algorithms with the powerful parallel processing capability of cloud computing to improve earthquake monitoring workflows. These efforts have helped to accelerate the development and improvement of machine learning models for earthquake monitoring.

REFERENCES

Aguilar, A. L. and G. C. Beroza (2023) Curated Regional Earthquake Waveforms (CREW) Dataset, *Seismica* (in revision).

Albuquerque Seismological Laboratory (ASL)/USGS (1980) US Geological Survey Networks [Data set], International Federation of Digital Seismograph Networks, doi:10.7914/SN/GS.

Brown, J. R., D. R. Shelly, and G. C. Beroza (2008) An autocorrelation method to detect low frequency earthquakes within tremor, *Geophys. Res. Lett.,* **35**, L16305, doi:10.1029/2008GL034560.

Burgess, M.K., and Roman, D.C., Ongoing (2015-) magma surge in the upper mantle beneath the island of Hawaii, *Geophys. Res. Lett.,* **48**(7), e2020GL091096, (2021).

Cole, H. M., W. L. Yeck, and H. M. Benz (2023) MLAAPDE: A Machine Learning Dataset for Determining Global Earthquake Source Parameters, *Seismol. Res. Lett.* **94**, pp. 2489–2499, doi: 10.1785/0220230021.

Fukuyama, E., Ellsworth, W. L., Waldhauser, F. & Kubo (2003) A. Detailed fault structure of the 2000 western Tottori, Japan, earthquake sequence. *Bull. Seismol. Soc. Am.,* **93**, pp. 1468–1478.

Gibbons, S. J. and Ringdal, F. (2006) The detection of low magnitude seismic events using array-based waveform correlation. *Geophysical Journal International* **165**, pp. 149–166.

Klein, F. W. (2002) User's guide to HYPOINVERSE-2000 a Fortran program to solve for earthquake locations and magnitudes, *USGS OFR* 02-171.

Kreps, J., Narkhede, N., and Rao, J. (2011) Kafka: a distributed messaging system for log processing, in *Proceedings of the NetDB,* **11**, pp. 1–7, Athens, Greece.

Kværna, T., D B Harris, S P Näsholm, A Köhler, S J Gibbons (2023) Tracking aftershock sequences using empirical matched field processing, *Geophys. J. Int.*, **235** (2) pp. 183–1200, doi.org/10.1093/gji/ggad297

Magrini, F., Jozinovic , D., Cammarano, F., Michelini, A., & Boschi, L. (2020) Local earthquakes detection: A benchmark dataset of 3-component seismograms built on a global scale, *Artificial Intelligence in Geosciences*, **1**, pp. 1–10.

Michelini, A., Cianetti, S., Gaviano, S., Giunchi, C., Jozinović, D., and Lauciani, V. (2021) INSTANCE–the Italian seismic dataset for machine learning, *Earth System Science Data*, **13**(12), pp. 5509–5544.

Mousavi, S. M. and C. A. Langston (2016) Hybrid seismic denoising using higher-order statistics and improved wavelet block thresholding, Bull. Seismol. Soc. Amer., 106 (4), pp. 1380–1393.

Mousavi, S. M. and C. A. Langston (2017) Automatic noise-removal/signal- removal based on general cross-validation thresholding in synchrosqueezed domain and its application on earthquake data,'' Geophysics, 82 (4), pp. 211–227.

Mousavi, S. M., and Beroza, G. C. (2020a) A machine-learning approach for earthquake magnitude estimation, *Geophys. Res. Lett.*, **47**, e2019GL085976. https://doi.org/10.1029/2019GL085976.

Mousavi, S. M. and G. C. Beroza (2020b) Bayesian-deep-learning estimation of earthquake location from single-station observations, *IEEE Transactions on Geoscience and Remote Sensing*, **58** (11), pp. 8211-8224, doi: 10.1109/TGRS.2020.2988770.

Mousavi, M. and G. C. Beroza (2022) Deep-Learning Seismology, *Science,* **377**, 607, doi:10.1126/science.abm4470.

Mousavi, M. and G. C. Beroza (2023) Machine Learning in Earthquake Seismology, *Annu. Rev. Earth. Planet. Sci.*, **51**, pp. 105-129.

Mousavi, S. M., W. Zhu, Y. Sheng, and G. C. Beroza (2019a) CRED: A Deep Residual Network of Convolutional and Recurrent Units for Earthquake Signal Detection, *Scientific Reports,* **9**:10267, https://doi.org/10.1038/s41598-019-45748-1.

Mousavi, S. M., Y. Sheng, W. Zhu, and G. C. Beroza (2019b) Stanford EArthquake Dataset (STEAD): A global data set of seismic signals for AI, *IEEE Access,* pp. 1-13, doi.org:10.1109/ACCESS.2019.2947848.

Mousavi, S. M., W. Zhu, W. L. Ellsworth, and G. Beroza (2020) Earthquake Transformer: An Attentive Deep-learning Model for Simultaneous Earthquake Detection and Phase Picking, *Nature Communications,* **11,** 3952, doi.org/10.1038/s41467-020-17591-w.

Pardo, E., Garfias, C. and Malpica, N. (2019) Seismic Phase Picking Using Convolutional Networks. *IEEE Transactions on Geoscience and Remote Sensing* (2019).

Ross, Z. E., Meier, M.-A., Hauksson, E. & Heaton, T. H. (2018) Generalized seismic phase detection with deep learning, *Bull. Seismol. Soc. Am.,* **108**, pp. 2894–2901.

ten Brink, U.S., Vanacore, E., Fielding, E.J., Chaytor, J.D., Lopez-Venegas, A.M., Baldwin, W.E., Foster, D.S., and Andrews, B.D. (2022) Mature diffuse tectonic block boundary revealed by the 2020 southwestern Puerto Rico seismic sequence, *Tectonics,* **41**(3), e2021TC006896.

University of Puerto Rico (1986) Puerto Rico Seismic Network & Puerto Rico Strong Motion Program, International Federation of Digital Seismograph Networks.

USGS Hawaiian Volcano Observatory (HVO) (1956) Hawaiian volcano ob- servatory network [Data set], International Federation of Digital Seismograph Networks, doi:10.7914/SN/HV.

Vanacore, E., von Hillebrandt Andrade, C., and McNamara, D.E. (2022) Preface to the SRL focus section on the 2020 southwestern Puerto Rico *M*w 6.4 earthquake and seismic sequence, *Seismol. Res. Lett.,* **93**, pp. 531–532.

Viltres, R., Nobile, A., Vasyura-Bathke, H., Trippanera, D., Xu, W., and Jonsson, S. (2022) Transtensional rupture within a diffuse plate boundary zone during the 2020 *M*w 6.4 Puerto Rico earthquake, *Seismol. Res. Lett.,* **93**, pp. 567–583.

Waldhauser, F. and Ellsworth, W. L. (2000) A double-difference earthquake location algorithm: Method and application to the northern Hayward fault, California. *Bull. Seismol. Soc. Am.,* 90, pp. 1353–1368.

Woollam, J., J. Münchmeyer, F. Tilmann, A. Rietbrock, D. Lange, T. Bornstein, T. Diehl, C. Giunchi, F. Haslinger, D. Jozinović, et al. (2022) SeisBench—A toolbox for machine learning in seismology, *Seismol. Res. Lett*., **93**, no. 3, pp. 1695–1709, doi: 10.1785/0220210324.

Yoon, C. E., O. O'Reilly, K. Bergen, and G. C. Beroza (2015) Earthquake detection through computationally efficient similarity search, S*ci. Adv.* **1**, e1501057.

Zaharia, M., Das, T., Li, H., Hunter, T., Shenker, S., and Stoica, I. (2013) Discretized streams: fault-tolerant streaming computation at scale, in *Proceedings of the 24th ACM Symp. Operating Systems Principles,* Farmington, Pennsylvania, USA, pp. 423–438.

Zhou, Y., Yue, H., Kong, Q. and Zhou, S. (2019) Hybrid Event Detection and Phase-Picking Algorithm Using Convolutional and Recurrent Neural Networks, *Seismol. Res. Lett.,* **90**, pp. 1079–1087.

Zhu, L., Z. Peng, J. McClellan, C. Li, D. Yao, Z. Li, L. Fang (2019) Deep learning for seismic phase detection and picking in the aftershock zone of 2008 Mw7. 9 Wenchuan Earthquake. *Phys. Earth Planet Int.,* doi: 10.1016/j.pepi.2019.05.004.

Zhu, W. and G. C. Beroza (2019) PhaseNet: A Deep-Neural-Network-Based Seismic Arrival Time Picking Method, *Geophys. J. Int.,* **216** pp. 261–273, doi:10.1093/gji/ggy423.

Zhu, W., K. S. Tai, S. Mostafa Mousavi, P. Bailis, and G. C. Beroza (2022) An End-to-End Earthquake Detection Method for Joint Phase Picking and Association using Deep Learning, *J. Geophys. Res.,* **127**, e2021JB023283. doi.org/10.1029/2021JB023283.

Zhu, W., A. B. Hou, R. Yang, A. Datta, S. Mostafa Mousavi, W. L. Ellsworth, and G. C. Beroza (2023) QuakeFlow: A Scalable Machine-learning-based Earthquake Monitoring Workflow with Cloud Computing, *Geophys. J. Int.,* **232**(1), 684, doi:10.1093/gji/ggac355.

Zhu, W., I. W. McBrearty, S. Mostafa Mousavi, W. L. Ellsworth, and G. C. Beroza (2022) Earthquake Phase Association using a Bayesian Gaussian Mixture Model, *J. Geophys. Res.,* **127***, e2021JB023249,* doi: 10.1029/2021JB023249, (2022).

Zhu, W., A. M. Mousavi, Y. Sheng, and G. C. Beroza (2019) Seismic Signal Denoising and Decomposition Using Deep Neural Networks, *IEEE Transactions on Geoscience and Remote Sensing*, **57**(11), pp. 9476-9488, doi:10.1109/TGRS.2019.2926772.

DISTRIBUTION LIST

DTIC/OCP
8725 John J. Kingman Rd, Suite 0944
Ft Belvoir, VA 22060-6218 1 cy

AFRL/RVIL
Kirtland AFB, NM 87117-5776 1 cy

Official Record Copy
AFRL/RVB/1st Lt. Simone E. Smith 1 cy